A TRIDENT SCHOLAR PROJECT REPORT

NO. 534

Nanomaterials-Based Liquid Crystal Devices for Improving their Stability and Electro-Optic Responses

by

Midshipman 1/C Derek T. Gess, USN

UNITED STATES NAVAL ACADEMY
ANNAPOLIS, MARYLAND

USNA-1531-2

REPORT DOCUMENTATION PAGE

Form Approved
OMB No. 0704-0188

1. REPORT DATE *(DD-MM-YYYY)*	**2. REPORT TYPE**	**3. DATES COVERED** *(From - To)*
5-16-23		

4. TITLE AND SUBTITLE
Nanomaterials-Based Liquid Crystal Devices for Improving their Stability and Electro-Optic Responses

5a. CONTRACT NUMBER

5b. GRANT NUMBER

5c. PROGRAM ELEMENT NUMBER

6. AUTHOR(S)
Derek T. Gess

5d. PROJECT NUMBER

5e. TASK NUMBER

5f. WORK UNIT NUMBER

7. PERFORMING ORGANIZATION NAME(S) AND ADDRESS(ES)

8. PERFORMING ORGANIZATION REPORT NUMBER

9. SPONSORING / MONITORING AGENCY NAME(S) AND ADDRESS(ES)
U.S. Naval Academy
Annapolis, MD 21402

10. SPONSOR/MONITOR'S ACRONYM(S)

11. SPONSOR/MONITOR'S REPORT NUMBER(S)
Trident Scholar Report no. 534 (2023)

12. DISTRIBUTION / AVAILABILITY STATEMENT

This document has been approved for public release; its distribution is UNLIMITED.

13. SUPPLEMENTARY NOTES

14. ABSTRACT

Liquid crystals (LC) are molecules that are used in display technology, commonly known as liquid crystal displays (LCDs). However, the LC materials contain free-ion impurities that stem from a variety of sources. These ionic impurities cause issues in electro-optic properties in current LCDs, such as slower response times and image-sticking effects. Ridding the LC cell of these ionic impurities can increase the electro-optic functionality of LCDs, allowing computer displays to function better. Two studies were conducted over the course of the project. The first study presents research showing that a small concentration of 50 nm-diameter gold nano-urchin (AuNUs) particles doped in the LC significantly reduces the concentration of free ions. The experiments showed a significant reduction in free-ion concentration, as well as an improvement in LC on-off switching time, rotational viscosity, and dielectric anisotropy. The second study was an extension of the first, where five more samples - utilizing 60 nm, 70 nm, 80 nm, 90 nm, and 100 nm-diameter AuNU - were synthesized at an optimal concentration acquired through the 50 nm AuNU experiments. Concentration and diameter-dependent study reveal a scientifically intriguing feature of the existence of an optimal concentration and diameter in which all tested properties of the LC were significantly improved.

15. SUBJECT TERMS
Liquid crystals, Gold nano-urchin particles, Ionic impurities, Image sticking

16. SECURITY CLASSIFICATION OF:			**17. LIMITATION OF ABSTRACT**	**18. NUMBER OF PAGES**	**19a. NAME OF RESPONSIBLE PERSON**
a. REPORT	**b. ABSTRACT**	**c. THIS PAGE**		32	**19b. TELEPHONE NUMBER** *(include area code)*

U.S.N.A. --- Trident Scholar project report; no. 534 (2023)

NANOMATERIALS-BASED LIQUID CRYSTAL DEVICES FOR IMPROVING THEIR STABILITY AND ELECTRO-OPTIC RESPONSES

by

Midshipman 1/C Derek T. Gess
United States Naval Academy
Annapolis, Maryland

Certification of Adviser Approval
Associate Professor Rajratan Basu
Physics Department

Acceptance for the Trident Scholar Committee
Professor Maria J. Schroeder
Associate Director of Midshipman Research

Table of Contents

1. Abstract

Liquid crystals (LC) are molecules with unique properties that allow them to be extensively employed in display technology, commonly known as liquid crystal displays (LCDs). However, LC develop free-ion impurities that stem from the LC chemical synthesis process, the LC cell's electrodes, and the organic polyimide alignment layers that are used to align the LC in a uniform direction. These ionic impurities cause issues in electro-optic properties in current LCDs, such as slower response times, short-term flickering, and long-term image sticking effects. Ridding the LC cell of these ionic impurities can increase the electro-optic functionality of LCDs, allowing computer displays to function better. Two studies were conducted over the course of the project. The first study presents research showing that a small concentration of 50nm gold nano-urchin (AuNUs) particles doped in the LC significantly reduces the concentration of free ions due to the spike-like formations that exist on the AuNU surface. These spikes trap the free ions within the LC solution, reducing their overall mobility. The experiments showed a significant reduction in free-ion concentration for some of the AuNU samples, as well as an improvement in LC on-off switching time, rotational viscosity, and dielectric anisotropy. This study also analyzes the effect of varying the concentration of AuNU particles on LCs and shows how an increase in AuNU concentration does not necessarily correlate to superior performance.

The second study was an extension of the first, where five more samples - utilizing 60nm, 70nm, 80nm, 90nm, and 100nm AuNU - were synthesized at the optimal concentration acquired through the 50nm AuNU experiments. Experiments run on each of these samples showed the effects that AuNU diameter has on the electro-optic functions of LC cells. This study also showed that an increase in LC diameter does not correlate with a decrease in free ion concentration. By performing various experiments on multiple concentrations, it was shown that an optimal concentration and diameter exist in which all tested properties were significantly improved.

2. Keywords

Liquid crystals, gold nano-urchin particles, ionic impurities, image sticking

3. Acknowledgments

This work was supported by the Office of Naval Research (Award No. N0001422WX02079) and the USNA Research Office. MIDN Gess would also like to thank his advisor, Dr. Rajratan Basu, for supporting his research interests over the past three years. Finally, he would like to thank the Trident committee for their support throughout the entirety of the Trident project.

4. Background

4.1. Liquid Crystal Properties

The term “liquid crystal” (LC) typically refers to a state of matter in which a material can flow like a liquid, but its molecules can align themselves in a relatively ordered structure, similar to a solid. LC materials are molecules with very specific properties. The first of such properties is that liquid crystals are long, ellipsoidal molecules. Because of their shape, chemical composition, and crystalline structure, these molecules have anisotropic properties, meaning that the properties of the molecules can change depending on their orientation. For example, LCs are considered birefringent, meaning they have two different indices of refraction: one along the major axis and one along the minor axis. This means that the transmittance of light through LC can change depending on the LC orientation [1].

Second, the chemical composition of liquid crystals is important. LCs typically have a dipole moment, which allows them to uniformly align in an electric field. An electric field is a region in which an electric force is exerted on a particle or object. In an LC cell, there exists a uniform electric field in which one side is positively charged and one side is negatively charged. Most LC are composed of a carbon-nitrogen (CN) bond, shown in Fig. 1, which is strongly polarized towards the nitrogen atom. This means that there is an uneven distribution of charge. Because of this uneven charge distribution, the LC can uniformly align themselves in the presence of an electric field, where the partial negative end is attracted to the positively charged plate and the partial positive end is attracted to the negatively charged plate. LCs also contain two benzene rings, which are hexagonal in shape, as seen in Fig. 1. These hexagonal rings assist in binding to surrounding LC molecules, as well as keeping orientation by binding to different layers in an LC cell. Finally, there are alkyl side chains attached to the end of the molecule which assist in elongating the LC to enhance its anisotropic properties [1], also seen in Fig. 1.

Because of the properties explained above, LCs have unique interactions with both light and electric fields and are widely used in modern computer display technology.

Figure 1: A schematic of an LC molecule, showing a carbon-nitrogen polar bond connected to two benzene rings, followed by a tail of alkyl side chains. The carbon-nitrogen bond gives the LC molecule its polarity, the benzene rings promote attraction between surrounding molecules, and the alkyl side chains assist in elongating the molecule in order to enhance its anisotropic properties.

4.2. *Light Polarization*

Visible light is a form of electromagnetic radiation – varying electric and magnetic fields that are perpendicular and oscillate at the same frequency and in phase with each other [2]. However, these fields' orientation is seemingly random when emitted from an unpolarized source, such as the sun or a lightbulb. Light polarization is essentially the process of filtering out only one of those orientations of light through the use of a polarizing material [2]. The various orientations go into the polarizing material, but only one orientation comes out, as seen in Fig. 2. It is important to note that, if a vertical polarizing filter is rotated 90˚ to the horizontal position and is stacked on top of another vertical polarizing filter, no light will be able to get through. The first filter polarizes the light in a horizontal orientation, but the second filter only allows vertically aligned light to pass through. Therefore, it results in no transmitted light, as shown in Fig. 4(a). However, due to certain properties of quantum mechanics that I will not cover in this paper, this is not true for filters that are rotated less than 90˚ out of phase. Examples of polarizing filters being used include in sunglasses to reduce the amount of sunlight that reaches the eye and in computer display screens, which will be explained in the next section.

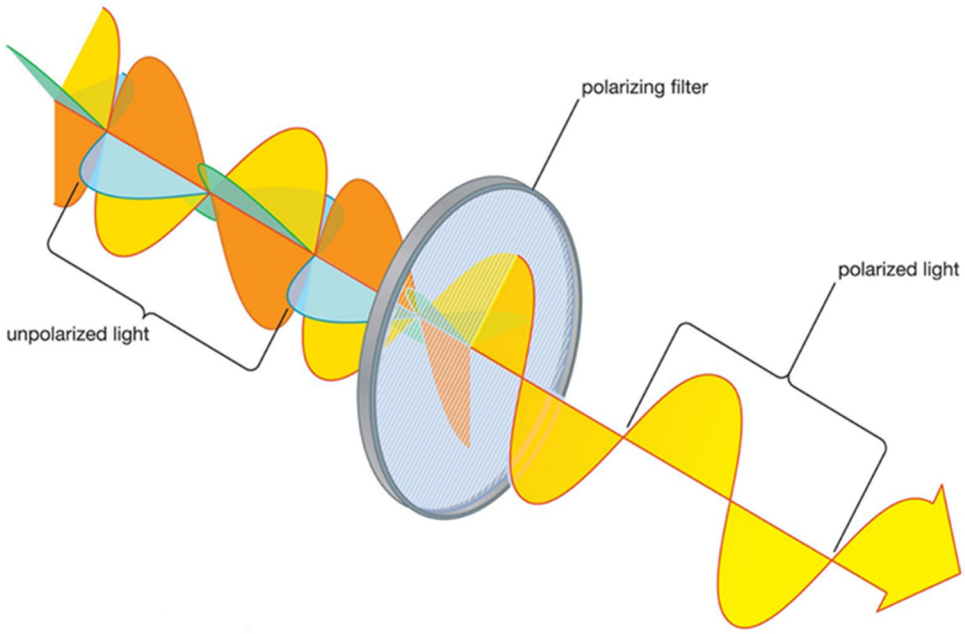

Figure 2: A schematic of unpolarized electromagnetic waves interacting with a polarizing filter. Only the wave orientation that matches the orientation of the polarized filter is able to pass through. All other orientations are either reflected or absorbed by the filter. Figure taken from: https://www.britannica.com/science/polarization-physics

4.3. *LC Use in Display Technology*

LC are commonly used in computer displays due to their unique intrinsic properties, as previously mentioned in Section 5.1. Fig. 3 below is a schematic of a singular pixel in a computer display screen comprising three subpixels with red, green, and blue filters. Millions of these pixels make up modern displays, typically called liquid crystal displays (LCDs). To understand how these molecules are integrated into the pixels, a brief understanding of the layers that make up the screen is necessary.

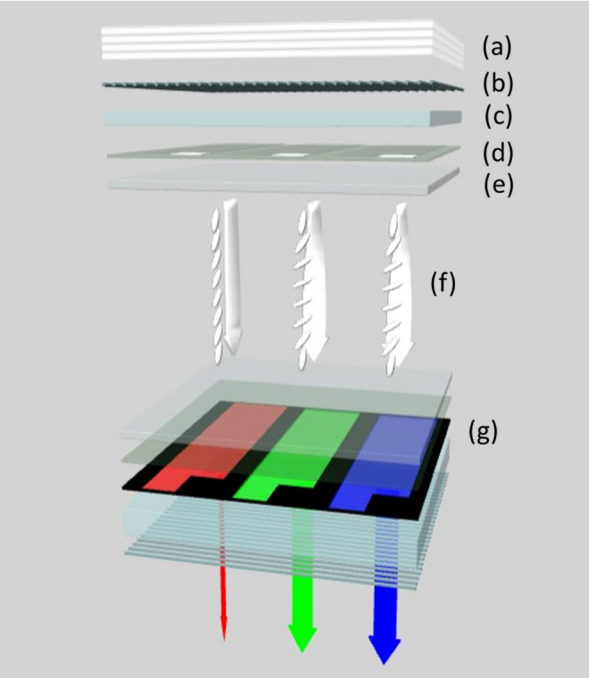

Figure 3: A schematic of the layers of an LC cell, from the top down: (a) shows the unpolarized light entering the cell. (b) is the initial vertical polarizer, polarizing the light in one orientation. (c) is the quartz substrate, which offers support for the LC cell. (d) is the electrode. (e) is the alignment layers. Its job is to align the LC in the same direction. (f) is where the liquid crystal solution exists. (g) is the layer that contains the red, green, and blue colored filters. There are duplicate layers (a), (b), (c), (d), and (e) on the bottom half of the cell. Figure taken from: https://downloads.emdgroup.com/lcd_explorer

Fig. 3 shows the various layers incorporated into a single pixel of a computer display. A pixel is made up of three LC cells, called subpixels. Each of the three subpixels in a pixel contains a different colored filter: either red, green, or blue (RGB), shown in Fig. 3(g). The importance of these subpixels will be explained later. First, there is a backlight, shown in Fig. 3(a), that exists behind the screen of the computer that emits unpolarized white light. This light passes through a vertically-aligned polarizer, Fig. 3(b), allowing only one orientation of the white light through.

The light passes through a series of transparent layers, including a quartz substrate (the backbone of the pixel) a transparent electrode, typically made out of the material indium tin oxide (ITO), and an alignment layer, typically made out of organic polyimide (PI), shown in Fig. 3(c), (d), and (e), respectively. Inside these layers is the LC solution. The job of the alignment layer is to keep the LC molecules oriented in the same direction when there is no electric field in the cell. In this orientation, the anisotropic properties of the LC molecules can be observed, as the light "twists" as it passes through the LC solution. On the other side of the solution, the light then goes through the same series of clear layers until it reaches the RGB filters. The once-white light has now switched colors to the color of its respective filter and travels through a horizontal polarizer to the eye of the user. While the light is now three different colors, the pixel is so small that the three colors mix together, appearing white to the user. The reason the light can pass through a vertical polarizer at the beginning and a horizontal polarizer at the end is due to the fact that the LC molecules "twisted" the orientation of the light so it was no longer vertically polarized, and was not impeded by the horizontal polarizer.

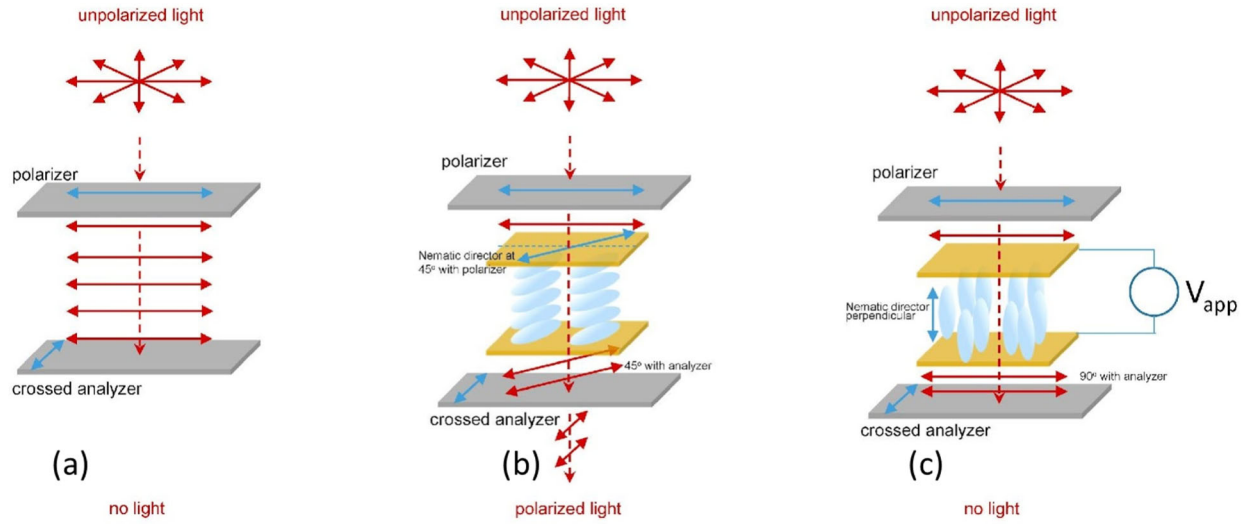

Figure SEQ Figure * ARABIC 4: (a) When unpolarized light travels through two crossed polarizers with no LC molecules in between, no light is transmitted. (b) When no external voltage is applied, there is no electric field, and E7 LC are horizontally aligned and allow light to transmit freely. When all of the light travels through the red, green, and blue filters, shown in Fig. 3, the color of the pixel appears white. (c) In the presence of an electric field, the LC molecules align to the electric field in the vertical orientation and transmit no light. Because no light is transmitted, the pixel appears black.

However, when a voltage is applied to the two electrodes in the pixel, an electric field is induced through the LC solution. Due to the molecule polarity, the LCs change their orientation to align with the field and are now oriented vertically. In this state, the LC molecules no longer "twist" the incoming light. Therefore, when the white backlight orients itself with the vertical polarizer, there is no intermediate layer that changes its orientation before it reaches the horizontal layer. Because of this, no light can be transmitted and the pixel is black. To change the color of the pixel, the voltage that is applied to each subpixel is varied to change the amount of light that can pass through the RGB filters, respectively. By varying the transmittance of RGB, one can create any color. Fig. 4(b) and (c) show the LC cell before and after a voltage is applied to the electrodes for E7 LC, the specific type of LC molecule that was used in the experiments.

4.4. Ion Impurities in LC Solutions

Excess ion impurities [3,4] in liquid crystals (LCs) present complications in electro-optic liquid crystal displays (LCDs), such as issues of image sticking [5-22]. Image sticking is a phenomenon where, when ions build up on the electrodes, they induce an internal electric field opposing the external electric field. This causes the liquid crystals to remain stagnant in their orientation, meaning that the pixels in the display are no longer changing colors. See Fig. 5. There is no way to fix this issue when the ions stay separated at the two opposite electrodes. Turning off the display does not immediately resolve this issue, as the separated ions still produce the internal electric field inside the pixels. When the display is turned off, the ions naturally relax into the LC, and the LC goes back to their normal state—this process can take several minutes to hours, depending on the ion concentration in the LC. Therefore, the internal electric field can be decreased by reducing free-ion concentration within the cell, and the LCs can operate properly.

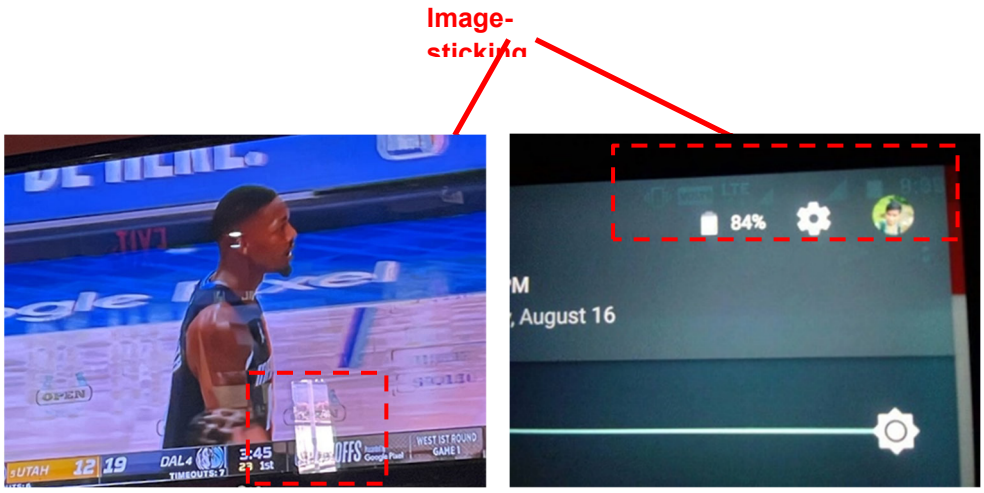

Figure 5: Two examples of image-sticking in LCD screens.

There currently exist processes to reduce the free-ion concentration during the chemical deposition process [23], such as chromatography, zone refining, recrystallizations, vacuum distillation, extraction, vacuum sublimation, ion exchange, and electrodialysis [24-28], but these existing solutions are time-consuming, expensive, and inefficient [24]. They also do not account for the free ions that may be introduced in the cell synthesis process from the electrodes and alignment layers [12-14]. New research involving various properties of nanomaterials [29-43] has proven to offer promising solutions to this prevalent issue. By doping LCs with nanomaterials, the overall performance of the LC device can be improved [37,44].

4.5. Gold Nano-Urchin Particles

Gold nano-urchins (AuNUs) [45], also coined gold nanoflowers or gold nanostars, are spike-like nanoparticles that have unique optical properties and can be utilized for sensor development, research purposes, and other applications [46]. In this paper, gold nano-urchins were used to decrease the number of free ions that exist in an LC solution. AuNUs have unique properties that allow them to be used in such an application. The free ions get trapped on the AuNUs because of the presence of asymmetric spike-like nano-urchins on the gold nanoparticle surface. Fig. 6(a) illustrates a schematic with free ions within an LC cell solution. Fig. 6(b) then illustrates the effect of the presence of AuNUs. The free ions are caught within the spikes and are unable to escape, rendering them no longer “free”. Fig. 6(c) shows an SEM image of an AuNU, clearly displaying the spike-like properties. There is no known attractive force between the AuNUs and the ions. The free ions get trapped on the AuNUs because of the presence of spikes on the surface gold nanoparticle.

The following experiments reveal that a significant reduction in free ions within the LC solution leads to improvements in intrinsic LC properties, such as rotational viscosity and dynamic electro-optic response times. The results also show an interesting relation between the concentration of AuNU and LC functional improvements – one that is not monotonic. There exists an optimal concentration, at which any concentration above or below will have poorer results. Finally, a relationship is observed between varying AuNU diameters and LC cell performance.

5. Experimental Section & Analysis

5.1. Sample Preparation

Varying diameters of 50, 70, 80, 90, and 100nm AuNU particles diluted in an ethanol solvent were purchased from NNCrystal US Corporation. Between the time of purchase and the synthesis of the AuNU-doped LC cell, the particles had aggregated together in the solution, causing an uneven concentration. To combat this, the ethanol+AuNU solutions were agitated by the process of sonication for two hours to evenly disperse the particles. The first solution of LC-E7 (EMD Millipore Corporation, T_{NI} = 60.0 °C) + 50nm AuNU was made at a concentration of 7.26×10^{-4} wt.% and subsequently named E7+AuNU1. Once mixed, this solution was sonicated for two hours in order to the dissolution of LC. The ethanol solvent was then evaporated to produce a pure LC+AuNU solution. The solution was finally degassed under a vacuum for five hours and sonicated until LC cell synthesis. This process was performed for three other concentrations of 50nm AuNUs in E7 LC: E7+AuNU2 = 13.4×10^{-4} wt.%, E7+AuNU3 = 24.8×10^{-4} wt.%, and E7+AuNU4 = 35.2×10^{-4} wt.%. A control cell was also created with just E7 LC. The test cells used in these experiments were commercially manufactured from Instec, Inc. (SA100A200uG180) with 1 cm^2 indium tin oxide (ITO) electrodes, a thickness of $d = 20\ \mu m$, and a 1.5° tilt angle. The cells were filled with the E7+AuNU solution at a temperature above 65°C to promote capillary action in the LC's isotropic phase. This sample preparation process was repeated to synthesize LC cells utilizing the other AuNU diameters concentrated around the concentration of LC+AuNU2 = 13.4×10^{-4} wt.%. These concentrations are as follows: E7+AuNU 70nm = 13.38×10^{-4} wt.%, E7+AuNU 80nm = 13.45×10^{-4} wt.%, E7+AuNU 90nm = 13.34×10^{-4} wt.%, and E7+AuNU 100nm = 13.46×10^{-4} wt.%.

Before the electro-optic experiments were conducted, the four known concentrations were analyzed under a cross-polarized microscope. Fig. 6(d), (e), (f), and (g) show the four concentrations of LC+AuNU. Fig. 6(h) shows the dotted rectangle in Fig. 6(g) at 10x magnification. A detailed explanation of these micrographs and their importance is discussed later.

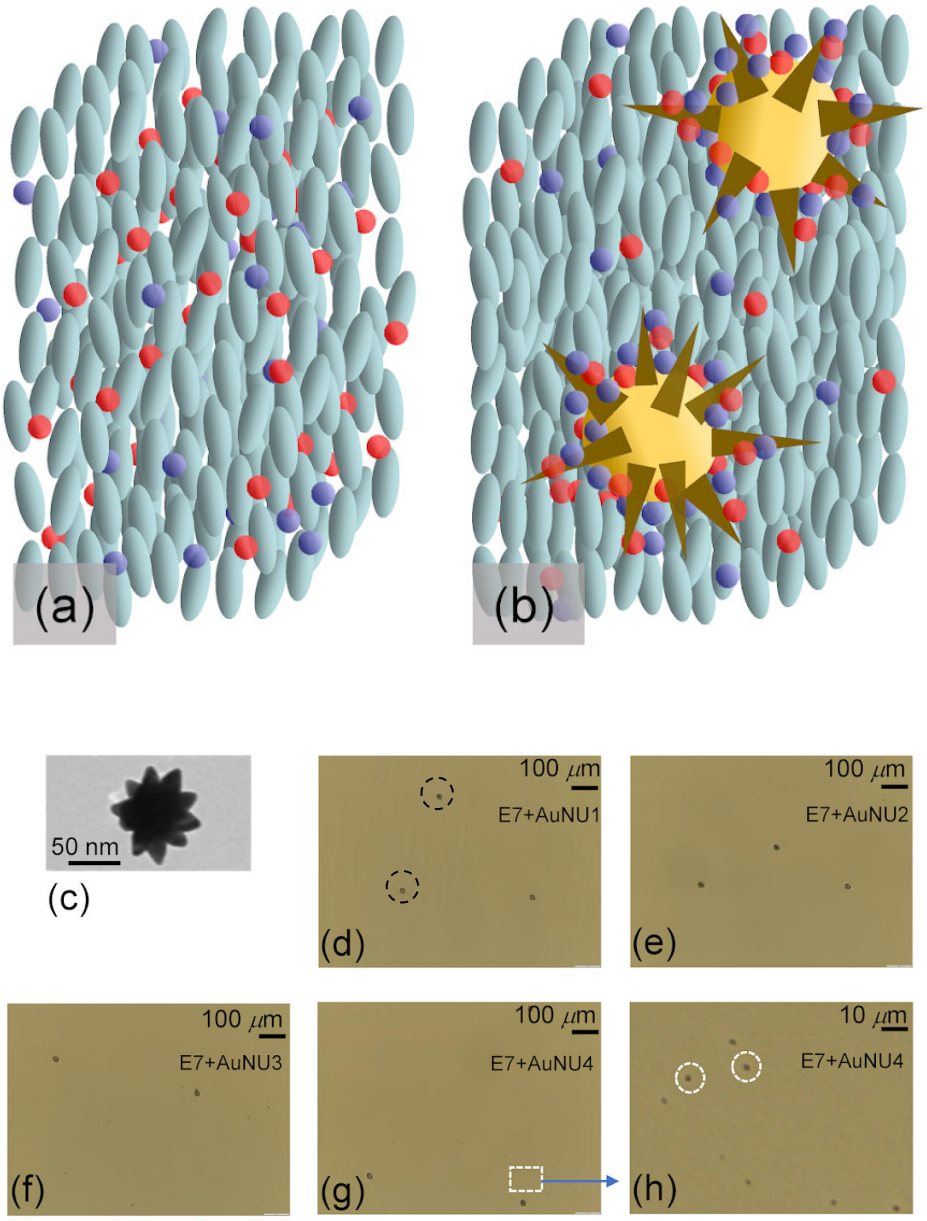

Figure 6: A schematic illustration of the presence of ions and AuNUs in the nematic phase. The small spheres represent the ions, the ellipsoids represent LC molecules, and the big spheres with spikes represent the AuNUs. (a) Random distribution of free ions in a nematic phase. (b) AuNUs' ion trapping process in a nematic phase. (c) An SEM image of an AuNU particle. Optical microphotographs under a cross-polarized microscope for (d) E7+AuNU1 (spacer particles shown in black), (e) E7+AuNU2, (f) E7+AuNU3, and (g) E7+AuNU4 samples. The 20 μm spacer particles from the LC cells are visible, and no AuNU aggregates are observed for E7+AuNU1 and E7+AuNU2. In addition to the spacer particles, several small aggregates are observed as small dark spots for E7+AuNU3 and E7+AuNU4. (h) A 10x magnified image of the dashed rectangular region of Fig. 5(g). Two such AuNU aggregates are shown in white two dashed circles. A scale bar is shown in each microphotograph.

5.2. Experiments on 50nm AuNU-Doped LC Cells

This paper describes four different experiments performed on all concentrations of E7 solutions doped with 50nm AuNU particles. Upon completion of the four experiments on the 50nm AuNU solutions, an optimal concentration of 13.4×10^{-4} wt.% was recognized. In order to test the effects of varying AuNU diameters on LC properties, this concentration was replicated for each of the available AuNU diameters (70nm, 80nm, 90nm, and 100nm).

5.2.1. Free-ion concentration

The free-ion concentration, n_i, in LC E7 and E7+AuNU mixtures was measured from the transient ion current, I_{ion} generated by inverting the polarity of the applied voltage across the cell [30,47]. When a square-wave voltage changing from +V to –V (*i.e.*, the voltage polarity is inverted) is applied across the cell, the LC molecules do not rotate as the director rotation depends only on the *magnitude* of the electric field *E*, and not on its *polarity* [50]. However, inverting the voltage polarity triggers the motion of the ions in the LC towards the opposite electrodes—which results in a transient ion current, I_{ion} in the cell. A square-wave peak-to-peak voltage of 20 V (*i.e.*, +10 V to –10 V) at 1 Hz was applied using an Automatic Liquid Crystal Tester (*Instec*, *Inc*.) to generate I_{ion} as a function of time in the test cells, as shown in Fig. 7(a) at T = 35 °C. This measurement was performed for all five samples but presented the I_{ion} only for the first three samples in Fig. 6(a) to keep the graph less crowded. Note that I_{ion} reaches its peak value when the positive and negative ions meet approximately at the middle of the cell. The peak time is defined by

$$t_{ion-peak} = \frac{d^2}{2\mu E} \tag{1}$$

where μ is the mobility [47], d is the cell-gap, and E is the electric field strength. Finally, I_{ion} decays to zero when the positive and negative ions reach the opposite electrodes—which can be seen in Fig. 6(a). The total free-ion transport in the test cells was then calculated by taking the area under the I_{ion} vs. time curve. The free-ion concentration,

$$n_i = (\int_0^t \quad I_{ion} dt)/(A \cdot d) \tag{2}$$

was extracted using the known cell-gap d and active area A of the cell. The uncertainty in n_i measurement is shown by the error bars in Fig. 7(b). At higher temperatures, the thermal energy provides kinetic energy to the ions within the solution. This increase in the kinetic energy of the ions allows more ions to emerge in the solution. Therefore, at higher temperatures, there are more ions, and the mobility of ions is larger. Fig. 7(b) presents n_i for all five samples as a function of

temperature, depicting that n_i is substantially suppressed for E7+AuNU1 and E7+AuNU2 compared to pure E7, even at higher temperatures. Note that n_i is suppressed by ~ 60% at the middle of the temperature range (45 ^oC) for the AuNU2 sample. Interestingly, n_i for E7+AuNU3 and E7+AuNU4 no longer decreases any further. In fact, n_i for E7+AuNU3 is higher than E7+AuNU1 and E7+AuNU2, but stays lower than pure E7. Moreover, n_i for E7+AuNU4 is very similar to that of the pure E7, indicating that this mixture does not effectively trap ions anymore. This issue will be addressed later from the AuNU-aggregation viewpoint. Note that there is no known attractive force between the AuNUs and the free ions. The free ions get trapped on the AuNUs because of the presence of asymmetric spike-like nano-urchins on the gold nanoparticle surface. Therefore, it is expected that the AuNUs trap both the positive and negative ions equally in the LC.

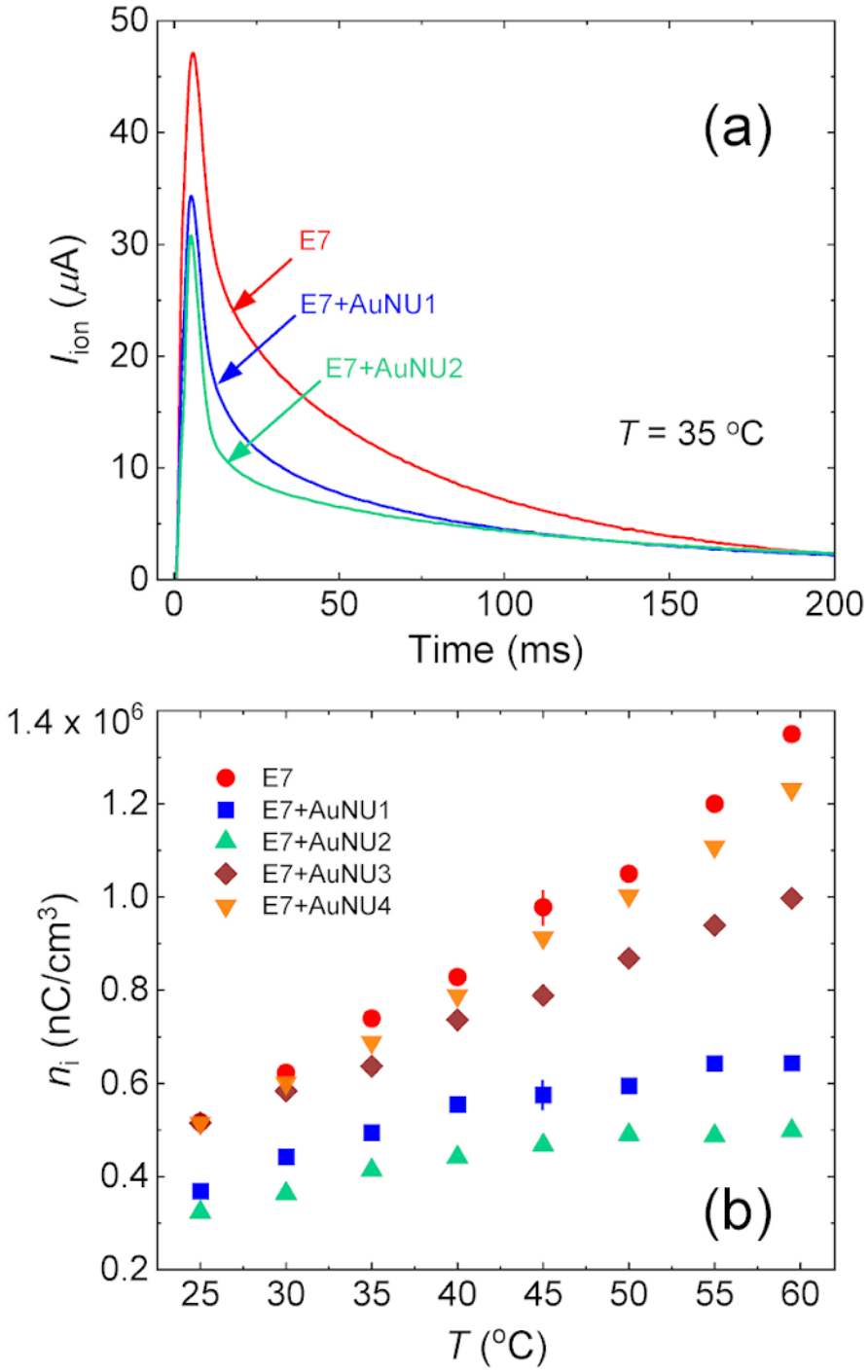

Figure 7: (a) Ion current, I_{ion} as a function of time for E7, E7+AuNU1, and E7+AuNU2 at 35 °C after the voltage is inverted across the cells. The peak represents the ion bump when positive and negative ions meet in the middle of the cell. (b) Free ion concentration, n_i, as a function of temperature for E7 and four different E7+AuNU samples listed in the legend. Typical error bars (uncertainties) are shown.

5.2.2. *Rotational Viscosity*

The following experiment was performed to determine rotational viscosity as a function of temperature. Rotational viscosity, γ_1 of an aligned LC, represents internal friction among LC molecules during the rotation process. The presence of excess free ions can greatly enhance this internal friction, increasing γ_1 of the LC [33]. We, therefore, performed experiments to study γ_1 the LC samples. The rotational viscosity for the nematic samples was obtained by measuring the transient current induced by a DC field across a planar-aligned capacitive-type cell configuration [48-50]. When a DC field (much higher than the threshold field) is applied across a planar LC cell, the induced current $I(t)$ through the cell shows a time response as the nematic director goes through the dynamic rotation. The current response is given by

$$I(t) = \frac{A\,(\Delta\varepsilon\,\varepsilon_o)^2\,E^3}{\gamma_1} sin^2[2\theta(t)] \tag{3}$$

where A is the area of the cell, E is the electric field, ε_o is the dielectric permittivity of free space, $\Delta\varepsilon$ is the dielectric anisotropy, and θ is the angle the director makes with the electrodes at a given time. At $\theta = 45^o$, $I(t)$ reaches its peak at the peak time,

$$t_p = [\frac{\gamma_1(-ln(tantan\,\theta_o))}{\Delta\varepsilon\,\varepsilon_o}]\,\frac{1}{E^2} \tag{4}$$

where θ_o is the pre-tilt angle. A DC field pulse with a pulse interval of 1 Hz was applied across the cell to generate $I(t)$. Then, $I(t)$ in the cell was detected as a function of time through a load resistor in series by a digital storage oscilloscope. The inset in Fig. 8(a) shows an example of $I(t)$ as a function of time for three different test cells, E7, E7+AuNU1, and AuNU2, at $T = 30^oC$. The peak current, I_p, was detected from the $I(t)$ vs. time graph to extract γ_1 from the known values of E, $\Delta\varepsilon$, and A. The uncertainty in γ_1 measurement is shown by the error bars in Fig. 8(a). The measurement of $\Delta\varepsilon$ is discussed later. Fig. 8(a) represents γ_1 as a function of temperature for the test cells listed in the legend. γ_1 shows the pre-transitional behavior for all the samples. Clearly, E7+AuNU1 and E7+AuNU2 exhibit a significant decrease in γ_1 compared to pure E7. In the temperature range from 25°C to 45°C, the average reduction in γ_1 for E7+AuNU2 is ~ 30%. Interestingly, E7+AuNU3 and E7+AuNU4 show an increase in γ_1.

There have been reports in the literature that suggest that the rotational viscosity of an LC decreases due to the suppression of ionic impurities. For example, a recent report [42] shows that the presence of quantum dots in an LC can suppress the ionic impurities—which causes a reduction in the overall ionic density and the resistance of the nematic medium. Consequently, the rotational viscosity of the quantum dot-doped LC system is reduced. Our group previously found [30] that graphene flakes can trap ionic impurities in a ferroelectric LC and reduce rotational viscosity. Another report in the literature [29] shows that Ti nanoparticles trap ions leading to stronger van

der Waals dispersion interactions between LC molecules and the alignment layers—which results in a smaller pre-tilt angle of the LC molecules at the alignment layers. From Eq. 4, $\gamma_1 \propto 1/(-ln(tan\ tan\ \theta_o))$, where θ_o is the pre-tilt angle. This equation suggests that when θ_o decreases γ_1 also decreases. We believe that due to the reduction of ionic impurities in the E7+AuNU1 and E7+AuNU2 samples, the internal resistance/friction is reduced, and the van der Waals dispersion interactions between LC molecules and the alignment layers are enhanced (hence a decrease in the pre-tilt angle). Thus, γ_1 is reduced in the two samples.

No quantitative theoretical model yet directly relates the ion concentrations to γ_1. However, we believe that reports in the literature mentioned above coherently suggest that the decrease in ionic impurities in the LC decreases γ_1, which is consistent with our results presented here.

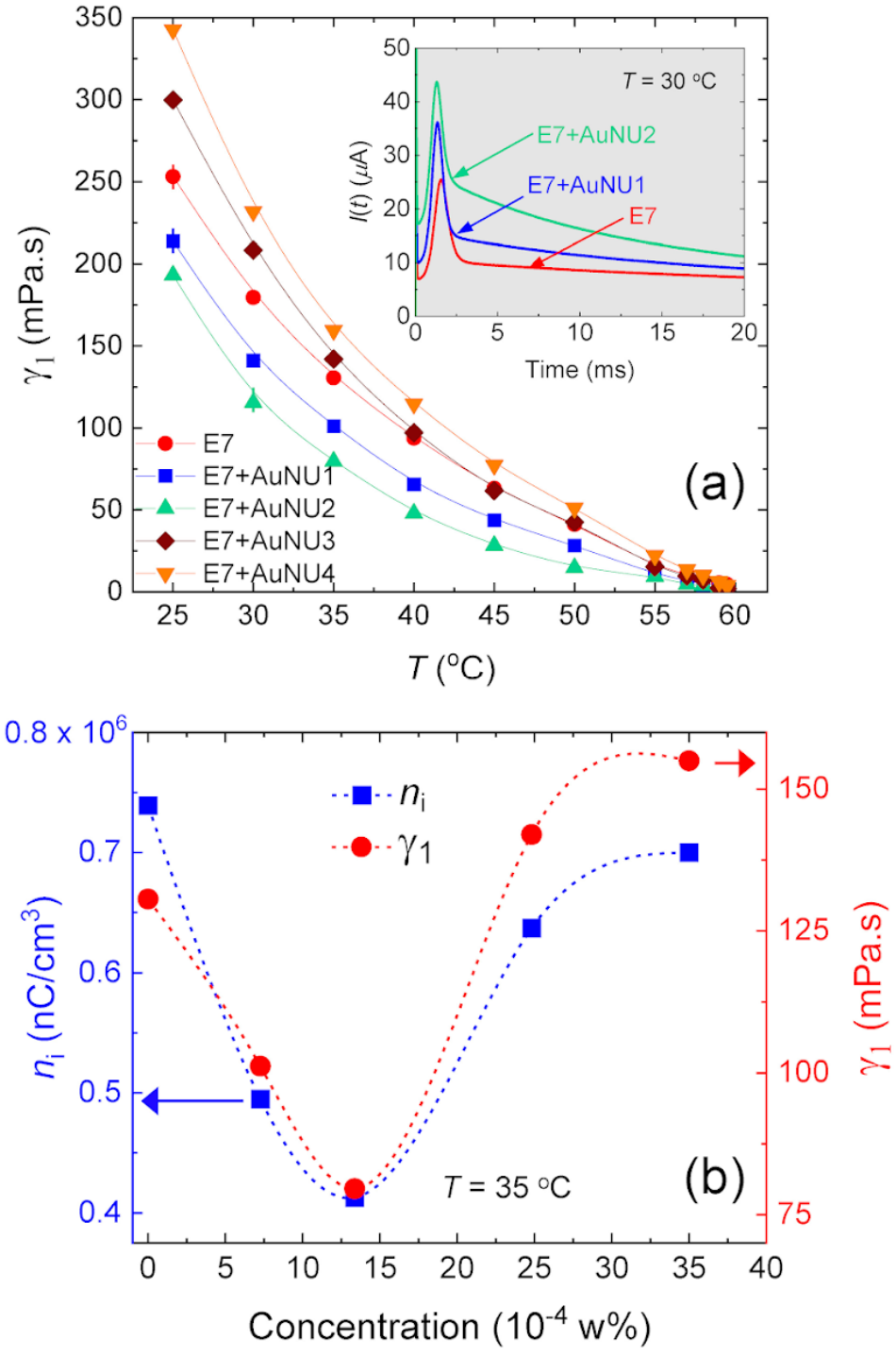

Figure 8: (a) Rotational viscosity, γ_1 as a function of temperature for E7 and four E7+AuNU samples, listed in the legend. Inset: Transient current, I(t) as a function of time for E7, E7+AuNU1, and E7+AuNU2 at T = 30 °C. Typical error bars (uncertainties) are shown. (b) γ_1 (right Y-axis) and n_i (left Y-axis) as a function of AuNU concentration at T = 35 °C. Dotted lines are a guide to the eye. An optimal concentration of E7+AuNU2 = 13.4 × 10^{-4} wt.% can be observed.

5.2.3. *AuNU Aggregation and Optimal Concentration*

Both n_i and γ_1 decrease for E7+AuNU1 and E7+AuNU2 and then increase for E7+AuNU3 and E7+AuNU4. This indicates that the E7+AuNU2 sample is the best or the most favorable concentration as far as the maximum decrease in n_i and γ_1 is concerned. This concentration is called the *optimal concentration*. Fig. 8(b) shows γ_1 (right *Y*-axis) and n_i (left *Y*-axis) as a function of AuNU concentration at T = 35ºC, depicting a clear correlation between n_i and γ_1. This correlation indicates that a decrease in n_i results in a reduction of γ_1. Also, note that two independent measurements, i.e., n_i and γ_1 indicate the same optimal AuNU concentration — E7+AuNU2.

The presence of the optimal concentration may be explained from the AuNUs aggregation viewpoint. As mentioned before, pure E7 and E7+AuNU samples were examined under a transmitted cross-polarized microscope. Pure E7, as expected, revealed a uniform nematic texture. Similarly, E7+AuNU1 and E7+AuNU2 exhibited uniform nematic textures, with no indication of phase separation or agglomerates of AuNUs at any temperature. See the micrographs in Figs. 6(d) and (e). Only 20 μm spacer particles are visible in the micrographs. So AuNUs are homogeneously distributed in the LC at low concentrations (E7+AuNU1 and E7+AuNU2). AuNUs start to aggregate when their concentration increases above E7+AuNU2 (*i.e.*, above the optimal concentration) in the LC. Figs. 6(f) and (g) show the microphotographs of E7+AuNU3 and E7+AuNU4 samples, respectively. A careful examination reveals that many small black dots are visible in addition to the 20 μm spacer particles in those micrographs. The white squared region in Fig. 6(g) is magnified 10x in Fig. 6(h), clearly showing several dark spots in E7+AuNU4. These dark spots are much smaller than the 20 μm spacer particles. These dark spots are identified as AuNU aggregates. Two such dark spots are highlighted using dashed circles in Fig. 6(h).

The AuNUs in aggregated form would not effectively suspend in the LC molecules and tend to phase-separate. Therefore, the aggregated AuNUs would not be effective in capturing ions. The AuNUs at high concentrations and in aggregated form in the LC media introduce some degree of internal friction, preventing us from getting the best out of the ion-trapping process. In other words, large aggregates can act as *external additives* and most likely increase the internal friction of the LC. We, therefore, believe that γ_1 starts to increase due to AuNU aggregation above the optimal concentration. For similar reasons, the changes in $\Delta\varepsilon$ are also observed.

5.2.4. *Dielectric Anisotropy*

The nematic phase shows dielectric anisotropy, $\Delta\varepsilon = \varepsilon_{||} - \varepsilon_{\infty}$, where $\varepsilon_{||}$ and ε_{∞} are the dielectric components parallel and perpendicular to the nematic director, respectively. An Automatic Liquid Crystal Tester (*Instec*, *Inc.*) was used to measure the dielectric constant ε as a function of the electric field at 1000 Hz for E7 and E7+AuNU samples utilizing the capacitance bridge technique [51]. Then, $\Delta\varepsilon$ was obtained from $\varepsilon_{||}$ and ε_{∞}. Fig. 9 demonstrates the temperature dependence of $\Delta\varepsilon$ for E7 and E7+AuNU samples. The inset in Fig. 9 shows $\Delta\varepsilon$ as a function of AuNU concentration at $T = 35^{o}$C. The uncertainty in $\Delta\varepsilon$ is shown by an error bar in the inset in Fig. 8. Clearly, $\Delta\varepsilon$ increases monotonically for E7+AuNU1 and E7+AuNU2, and then it starts to decrease for E7+AuNU3 and E7+AuNU4. The result shown in the inset in Fig. 8 also independently exhibits the presence of the *optimal concentration*, E7+ AuNU2, for the enhancement in $\Delta\varepsilon$. It has been shown that reducing ion impurities can enhance the overall anisotropy of the LC and $\Delta\varepsilon$ increases subsequently [42,43]. This is consistent with the first two concentrations, E7+AuNU1 and E7+AuNU2. At higher concentrations, when AuNUs aggregate in the LC, they locally disrupt the nematic order. The dielectric anisotropy $\Delta\varepsilon$ is proportional to the order parameter. Therefore, $\Delta\varepsilon$ is observed to decrease for E7+AuNU3 and E7+AuNU4.

According to Maier and Meier's theory [53], the dielectric anisotropy $\Delta\varepsilon$ is given by

$$\Delta\varepsilon = \frac{NhFS}{\varepsilon_o}\left[\Delta\alpha + \frac{\mu_{LC}^2 F}{2k_B T}(3cos^2\beta - 1)\right] \quad (5)$$

where N is the number density, h is the cavity field factor, F is the feedback factor, S is the order parameter, μ_{LC} is the dipole moment of the LC, $\Delta\alpha$ is the polarizability anisotropy, k_B is the Boltzmann constant, T is the temperature, and β is the angle between the long molecular axis and the dipole moment of LC molecules [53].

In the presence of free ions, LC molecules tend to collect charges on their ends due to their polar nature: the partial positive side accumulates negative ions and the partial negative side accumulates positive ions. See Fig. 10. The positive and negative ions are separated by a distance similar to the length of the molecule, which induces a dipole moment μ_{ion} in the opposite direction of the LC's dipole moment μ_{LC}. These two dipole moments subtract, resulting in the resultant dipole moment $\mu_{effective} = \mu_{LC} - \mu_{ion}$. By decreasing the number of free ions, the number of accumulating ions on the LC molecule decrease, therefore reducing the opposing dipole moment and increasing the value of $\mu_{effective}$. When $\mu_{effective}$ increases, so does $\Delta\varepsilon$, as shown by equation (5).

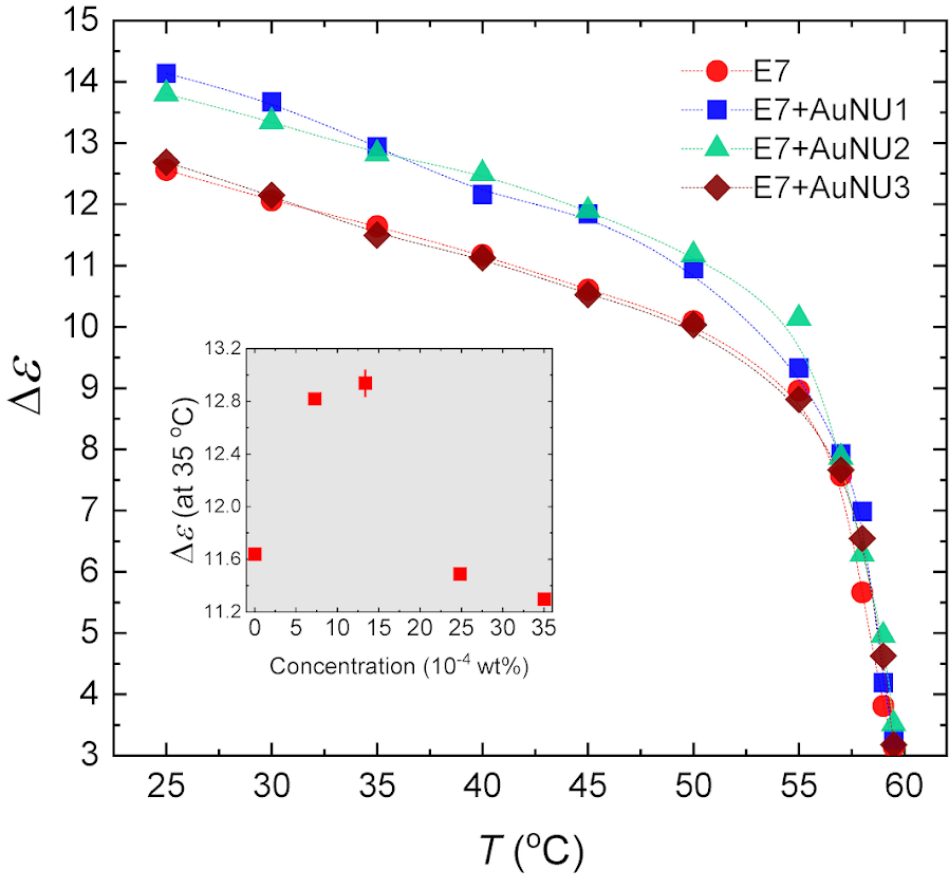

Figure 9: Dielectric anisotropy, ⊗∑ as a function of temperature for E7 and E7+AuNU samples, listed in the legend. Inset: Dielectric anisotropy, ⊗∑ as a function of AuNU concentration at T = 35 °C. A typical error bar is shown.

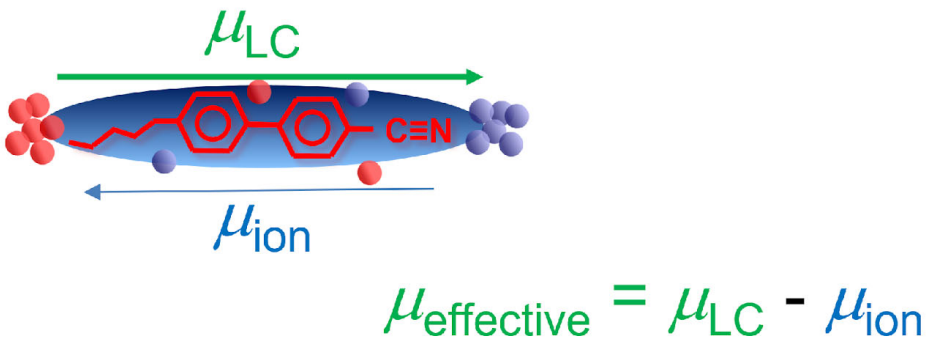

Figure 10: A schematic representation of the dipole moment of the LC, μ_{LC}, and the dipole moment due to the ion accumulation, μ_{ion}.

The number density of the free ions in the LC E7 is ~ 10^{16}/cm^3 (from Fig. 7(b)). The number density of the doped AuNUs in the LC is ~ 10^9/cm^3 (determined from an AuNU particle mass, $m_{AuNU} = 1.27 \times 10^{-15}$ g). Also, the ions are much smaller in size than the AuNUs. Thus, the ions can effectively accumulate around the LC molecules due to their large number density and smaller size and, then, can affect the polarity of the LC molecules. The AuNUs, on the other hand, cannot affect the polarity of the LC molecules since the AuNUs are neutral. Therefore, the AuNUs, in non-aggregated forms, do not change the LC characteristics significantly.

At higher concentrations (E7+AuNU3 and E7+AuNU4), when AuNUs aggregate in the LC, they no longer effectively trap ions. Therefore, $\Delta\varepsilon$ does not increase any further for these two higher concentrations. In aggregated forms (E7+AuNU3 and E7+AuNU4), we believe the AuNUs distort the nematic director field locally, and the overall orientational order decreases slightly. Consequently, the order parameter S also decreases. The dielectric anisotropy $\Delta\varepsilon$ is proportional to S, according to Eq. 5. Therefore, a slight decrease in $\Delta\varepsilon$ for E7+AuNU3 and E7+AuNU4 is observed.

5.2.5. *Electro-Optic Switching Response*

The rotational viscosity, γ_1, is linearly proportional to the dynamic electro-optic response of an aligned nematic LC. Since γ_1 is significantly altered for the E7+AuNU samples, the dynamic electro-optic response of these hybrid samples was studied and compared with the pure E7. The dynamic electro-optic response was studied using an optical setup with a 5-mW He-Ne laser beam (λ = 633 nm) sent through a polarizer, the LC cell (where the director was oriented at 45° with respect to the polarizer), a crossed analyzer, and into a photodetector. The output of the photodetector was connected to a digital storage oscilloscope to detect the change in the transmitted intensity through the cell as a function of time when a square-wave voltage of 30 Hz was applied across the cell. See Fig. 9. Transmittance responses were studied for several applied voltages much higher than the orientation threshold switching voltage, V_{th}, at T = 20°C. In Fig. 10(a), the left y-axis represents the normalized transmitted intensity of LC E7, E7+AuNU1, and E7+AuNU2 as a function of time when a square-wave voltage (40 V) was turned off. Similarly, in Fig. 10(b), the left y-axis represents the normalized transmitted intensity of the same three samples as a function of time when the square-wave voltage (40 V) was turned on. After the voltage is turned on, the transmitted intensity through the cell decreases. The time it takes to drop from 90% to 10% of its maximum value is defined as the optical switching on, τ_{on}. After the voltage is turned off, the transmitted intensity increases, and the optical switching off, τ_{off} is defined by the time it takes to rise from 10% to 90% of its maximum value. These two switching times, τ_{on} and τ_{off} are described as [52]

$$\tau_{on} \propto \frac{\gamma_1 d^2}{\Delta\varepsilon\, \varepsilon_o V^2 - K_{11}\pi^2}; \quad \tau_{off} \propto \frac{\gamma_1 d^2}{K_{11}\pi^2} \tag{3}$$

where γ_1 is the rotational viscosity, d is the cell-gap, $\Delta\varepsilon$ is the dielectric anisotropy, V is the applied voltage, ε_0 the is free space permittivity, and K_{11} is the splay elastic constant.

Figs. 11(a) and 11(b) show τ_{off} and τ_{on}, respectively, for the samples as a function of applied voltage, V. The uncertainties in τ_{off} and τ_{on} are shown by error bars. Clearly, τ_{off} and τ_{on} are both faster for E7+AuNU1 and E7+AuNU2 compared to that of the pure E7. Note that the switching off, τ_{off} is ~ 35% faster, and the switching on, τ_{on} is ~ 33% faster for the E7+AuNU2 sample compared to the pure E7. A reduction of free ions lessens γ_1 in those two samples—which governs this faster response. At the higher concentrations, γ_1 is increased due to the AuNU-aggregations; therefore, the electro-optic switching is slower. The dynamic response of the E7+AuNU3 sample is not shown in Fig 10(a) and 10(b) to keep the figures less crowded. Only τ_{off} and τ_{on} for this concentration are shown in Figs. 11(a) and 11(b) for proper comparison. Since the response times for the E7+AuNU3 sample are already higher than the pure E7, this dynamic electro-optic study for the E7+AuNU4 sample was not conducted, knowing that it will also show a slower response.

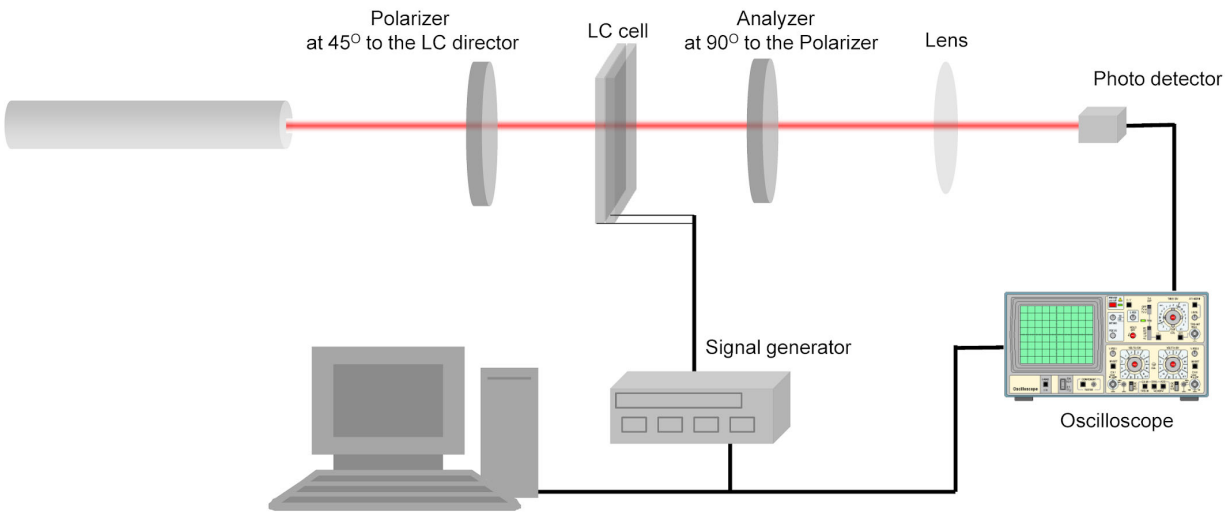

Figure 10: The electro-optic experimental setup for measuring τ_{off} and τ_{on}. The 5-mW He-Ne laser beam (shown in the top left), sends a monochromatic beam through a polarizer, the LC cell, and an analyzer angled at 90˚to the polarizer. A photodetector picks up the transmitted light signal and converts the light signal into a voltage, which is read by the oscilloscope.

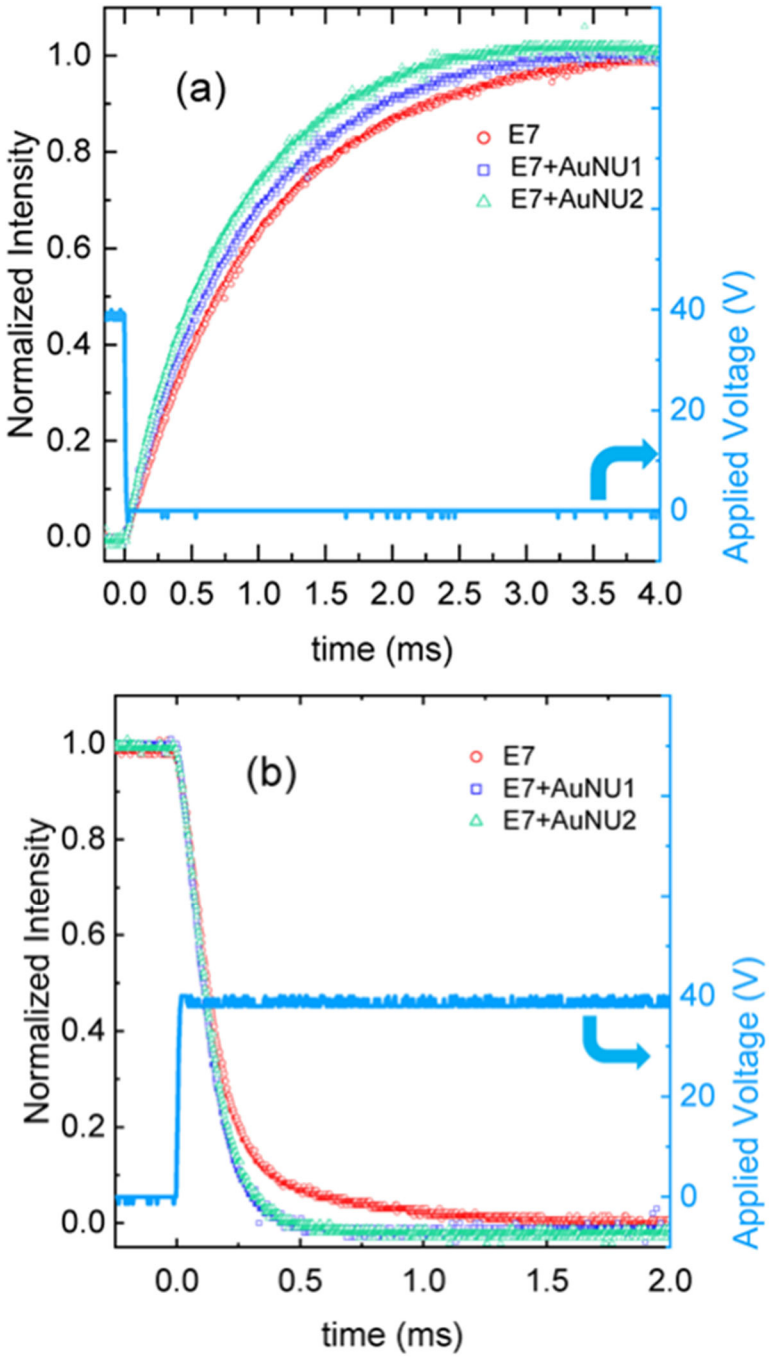

Figure 5: Dynamic electro-optic switching of E7 and E7+AuNU samples. (a) The left *Y*-axis shows the normalized transmitted intensity (unitless) as a function of time when a 40 V applied voltage is turned off, for the test cells listed in the legend ($T = 20^{o}$ C). The right *Y*-axis shows the applied voltage profile. (b) The left *Y*-axis shows the normalized transmitted intensity as a function of time when a 40 V applied voltage is turned on, for the test cells listed in the legend ($T = 20^{o}$ C). The right *Y*-axis shows the applied voltage profile.

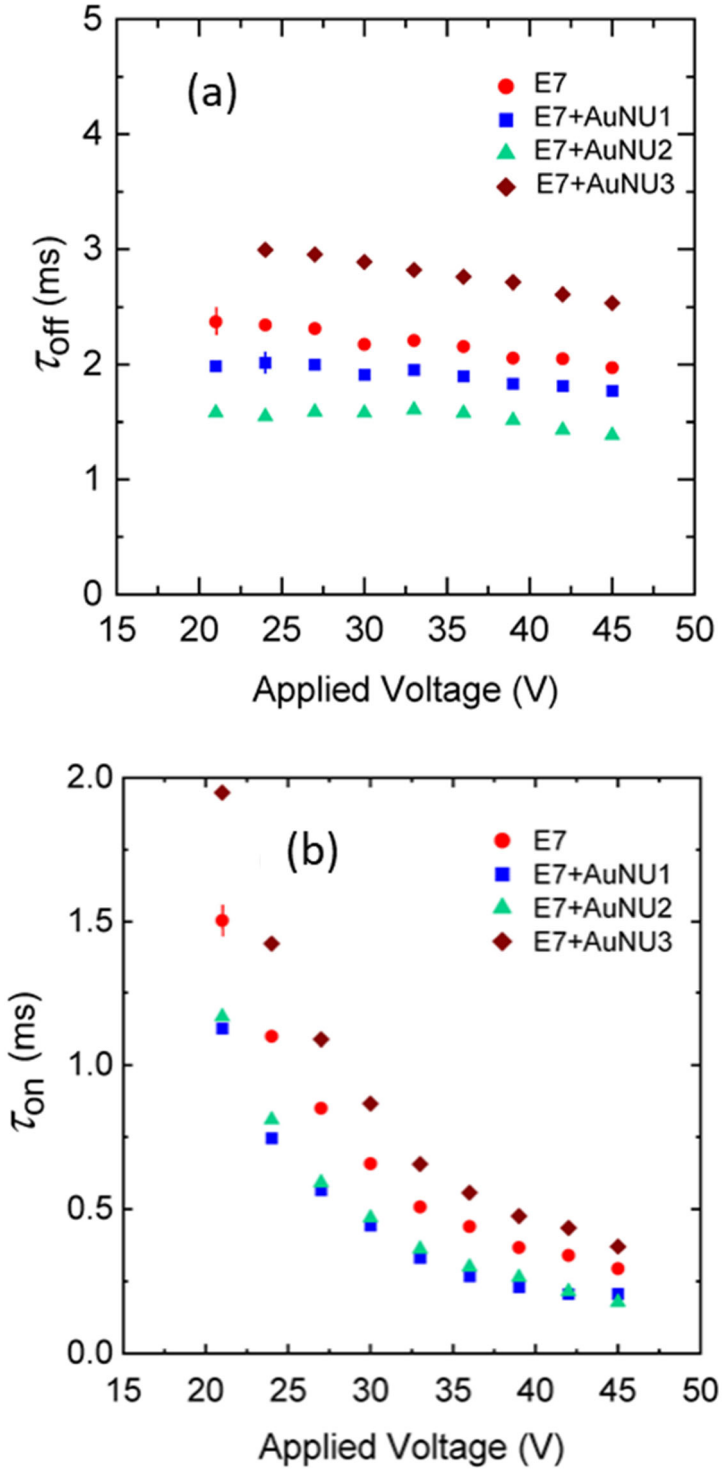

Figure 12: (a) Optical switching off, τ_{off}, and (b) optical switching on, τ_{on} as a function of applied voltage for E7 and E7+AuNU samples listed in the legend. Typical error bars (uncertainties) are shown.

5.3. Experiments on Varying AuNU Diameters at Constant Concentration

In Fig. 8(b), a correlation between free ion concentration and rotational viscosity can be observed. The concentration of 50nm AUNU that optimizes both of these experimentally measured properties is E7+AuNU2, which was synthesized at a concentration of 13.40×10^{-4} wt.%. In order to test the effects that AuNU diameter size has on free ion concentration and rotational viscosity, γ_1, samples utilizing four different diameters of 70 nm, 80 nm, 90 nm, and 100 nm were synthesized and the experiments to measure these values were carried out, starting with a measurement of free ion concentration. The setup and subsequent experiment match the description given in section 5.2.1. The results for this experiment are given in Fig. 13(a), displaying a fairly substantial decrease in free ion concentration across all five measured diameters. However, E7+AuNU 80nm performed the best over the measured temperature range, showing an ~85% decrease in free ions at the lowest measured temperature of 25˚C and an ~80% decrease at the middle of the temperature range (45℃) within the solution. The difference between E7+AuNU 80 nm's free ion concentration compared to the other measured samples suggests there is a correlation between AuNU diameter size and their ability to trap free ions, reducing their mobility within the solution. We suggest that 80nm is the largest AuNU diameter that can be suspended in E7 LC solutions before they either begin to aggregate, as we saw in the higher 50nm AuNU concentrations, or sink to the bottom of the cell. The reason a larger particle diameter is ideal is that it increases the amount of surface area available to trap ions. At the ideal concentration established in the 50nm experiments, 80nm AuNU particles are the largest particles that can achieve this.

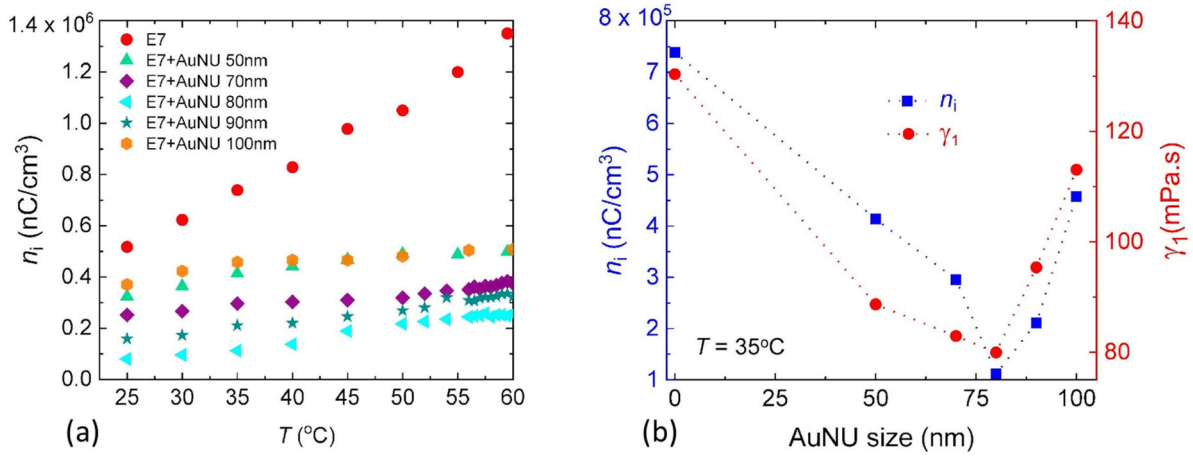

Figure 13: (a) Free ion concentration, n_i, as a function of temperature for E7 and five different E7+AuNU samples with varying diameters, shown in the legend. The graph shows that E7+AuNU 80nm outperformed the other E7+AuNU samples, decreasing the free ion concentration in the LC solution by ~80%. (b) γ_1 (right Y-axis) and n_i (left Y-axis) as a function of AuNU diameter size at $T = 35$ °C. Dotted lines are a guide to the eye. An optimal 80nm diameter size can be observed.

The experiment to measure rotational viscosity, γ_1, was performed next, following the setup and experimental method given in section 5.2.2. γ_1 is a measure of the internal friction of the LC during their rotation process. When free ions are introduced to an LC solution, the ions impede the motion of the LC while they are rotating, increasing the internal friction and therefore increasing γ_1. Fig. 13(b) shows γ_1 (right Y-axis) and n_i (left *Y*-axis) as a function of AuNU diameter size at T = 35˚F and shows a clear correlation between γ_1, n_i, and AuNU diameter size. The graph indicates that E7+AuNU 80 nm is the ideal diameter of the measured diameters. It also confirms the conclusions in section 5.2.3 that a decrease in n_i results in a subsequent reduction in γ_1.

It is important to mention that experiments to test the electro-optic switching effect and dielectric anisotropy were also carried out on all four diameters, but the results did not add a new understanding of the effect that AuNUs have on these measurements. Therefore, that data was not included in this report.

Nanomaterials	Concentration in LC	Ion Trapping Ability
Gold Nanoparticles (without urchins)	~0.1 wt.%	none
Graphene Nanoplatelets	~0.5 wt.%	30%
Fullerenes, C_{60}	~0.5 wt.%	80%
Ferroelectric Nanoparticles ($BaTiO_3$)	~0.275 wt.%	50%
Titanium Dioxide (TiO_2)	~0.1 wt.%	53%
Gold NanoUrchins (AuNUs)	~10^{-3} wt.%	80%

Table 1: A table comparison of AuNU concentration and subsequent ion trapping ability as compared to other nanomaterials. The ion trapping ability shows the percent reduction in free ions within the LC solution.

Table 1 compares AuNUs to other nanomaterials with ion-trapping abilities. AuNUs had the highest percentage of free ion reduction out of the listed nanomaterials, with an ion trapping ability of 80%. Compared to fullerenes, the material with similar ion trapping abilities, the required doping concentrations to achieve the same ion trapping results was ~100 times less for AuNUs. Fewer particles doped in the LC solution correlates to decreased rotational viscosity, increased dielectric anisotropy, and decreased on-off electro-optic switching times [24,30].

6. Conclusion

It is experimentally demonstrated that a small quantity of AuNUs in the LC can lower the LC's free ion concentration by the ion trapping process. Our AuNU concentration-dependent study indicates that there exists an optimal concentration of AuNUs, above which the ion-trapping by the dispersed AuNUs is not significant. Below or at the optimal concentration (E7+AuNU1 and E7+AuNU2), where the ion-trapping by the dispersed AuNUs is more effective, the presence of the free ions is significantly (~60%) suppressed. The presence of fewer mobile ions decreases the internal friction of the nematic media, enabling the nematic director to rotate faster. Therefore, the rotational viscosity was observed to decrease below the optimal concentration. However, being embedded in the LC, the AuNUs themselves act as external additives and can increase the internal friction in the LC. Therefore, in one way, the reduction of free ions tends to decrease the rotational viscosity, and in the other way, higher AuNU concentrations tend to increase the rotational viscosity. When the concentration of AuNUs increases above a specific limit (optimal csconcentration), they aggregate and rapidly enhance the internal friction of the LC. The presence of AuNUs at higher concentrations (E7+AuNU3 and E7+AuNU4) overmatches the impact of the reduction of ions on the rotational viscosity. Consequently, the rotational viscosity was observed to increase above the optimal concentration. It is also experimentally shown that the decrease of free ions and the lower rotational viscosity, below the optimal concentration, resulted in an accelerated electro-optic response of the LC.

It is also shown that AuNU diameter has a noticeable effect on the free ion concentration and rotational viscosity in LC solutions when doped at a constant concentration. While all tested diameters had a positive effect in reducing free ion concentration and rotational viscosity, the results suggest that there exists an optimal diameter between 50 nm and 100 nm that minimizes the negative effects that these physical properties have on liquid crystal displays. Our experiments showed that E7+AuNU 80nm was the optimal diameter, reducing the free ion concentration in the LC solution by ~80%, significantly suppressing all consequences of free ion impurities. The 80nm AuNU diameter is optimal, most likely because it is the largest particle that can be suspended in an LC solution without aggregating. The consequences of larger particles forming aggregates are that they interfere with the LC's ability to move freely within the LC cell. The 80 nm AuNU particles have a larger effective surface area to trap free ions compared to the smaller diameter particles, which contribute to the superior performance in ion concentration reduction and consequent superior performance in properties such as rotational viscosity, electro-optic switching, and dielectric anisotropy.

These results are important for purifying LCs from excess ionic impurities, and concentration-dependent studies and diameter-dependent studies reveal a scientifically intriguing feature of the existence of an optimal concentration and diameter.

The original description of this Trident Scholar project involved two projects: one to test the optical transmission effects of vertically aligned carbon nanotubes (VA-CNT) in a hybrid aligned nematic LC cell and the second to test the effect that AuNU diameter has on free ion concentration. However, because my SP496 research project involved preliminary experiments on 50nm AuNU-doped LC solutions, my advisor and I decided it would be best to continue the AuNU experiments for continuity. Initially, the AuNU-based project was oriented only around varying diameters; however, we performed experiments to measure four different measurements on five different concentrations of 50nm AuNU-LC solutions in order to study the effect that concentration has on free ion concentration. These experiments were time-consuming and very difficult to perform. The entire process of synthesizing the cell and performing each experiment took about a week and a half if everything went smoothly. Of course, laboratory work is never perfect, and we encountered some equipment issues along the way. However, the first semester of the Trident project was dedicated solely to studying the effects of concentration on AuNU diameter as well as writing a paper to submit to *Physical Review E* from the American Physical Society (APS) for publication and developing deliverables for the Trident committee. The second semester was dedicated to studying the effects of changing AuNU diameter on free ion concentration. We performed the same experiments on five different diameters of AuNU doped at a constant concentration. Again, these experiments took about 1.5 weeks per diameter to complete. During this time, we were also preparing a presentation for the APS March Meeting 2023 in Las Vegas, NV.

The AuNU project has significantly advanced the field of soft condensed matter physics. The project has allowed us to conduct systematic research on novel nanomaterial-based transmissive LC devices to achieve improved efficiency (*i.e.*, reduction of ion impurities) and enhanced tunability (*i.e.*, faster electro-optic switching). The success of this research project has led to understanding the nanoscale interfacial interactions between LC and nanomaterials materials at a much deeper level. The results have also successfully bridged the gap between the ‘fundamental LC-nanomaterial interactions’ and ‘designing nanostructure-based photonic LC devices’. Therefore, the performed experiments have potential applications in display technology. Our paper on this project has already been published in Physical Review E with excellent review comments. While the VA-CNT project would have been an interesting study, the AuNU project proved to be both a challenging and rewarding Trident Scholar project.

Peer-review publication from this project:

R. Basu and D.T. Gess, "*Ion trapping, reduced rotational viscosity, and accelerated electro-optic response characteristics in gold nano-urchin—nematic suspensions*," **Physical Review E 107, 024705 (2023)**. PDF link

PHYSICAL REVIEW E **107**, 024705 (2023)

Ion trapping, reduced rotational viscosity, and accelerated electro-optic response characteristics in gold nano-urchin–nematic suspensions

Rajratan Basu * and Derek T. Gess
Department of Physics, Soft Matter and Nanomaterials Laboratory, The United States Naval Academy, Annapolis, Maryland 21402, USA

(Received 18 November 2022; accepted 13 February 2023; published 27 February 2023)

The free-ion concentration in a nematic liquid crystal (LC) is found to be significantly reduced when gold nano-urchins (AuNUs) of 50-nm diameter are dispersed in the LC in dilute concentrations. The nano-urchins on AuNUs trap a significant amount of mobile ions, reducing the free-ion concentration in the LC media. The reduction of free ions results in a decreased rotational viscosity and accelerated electro-optic response of the LC. The study is carried out with several AuNUs concentrations in the LC, and the experimental results consistently suggest that there exists an optimal concentration of AuNUs, above which they tend to aggregate. At the optimal concentration, the ion trapping is maximum, rotational viscosity is at its lowest, and the electro-optic response is the fastest. Above this optimal AuNUs concentration, the rotational viscosity is found to increase, and consequently, the LC no longer exhibits an accelerated electro-optic response.

DOI: 10.1103/PhysRevE.107.024705

7. References

[1] Lower, Stephen. "Liquid Crystals." LibreTexts Chemistry. January 30, 2023.

[2] Britannica, T. Editors of Encyclopaedia. "Polarization." *Encyclopedia Britannica*, December 23, 2022.

[3] G. H. Heilmeier and P. M. Heyman, "Note on Transient Current Measurements in Liquid Crystals and Related Systems," Phys. Rev. Lett. 18(15), 583-585 (1967).

[4] G. Briere, F. Gaspard, and R. Herino, "Ionic residual conduction in the isotropic phase of a nematic liquid crystal," Chem. Phys. Lett. 9(4), 285-288, (1971).

[5] S. Takahashi, "The investigation of a dc induced transient optical 30-Hz element in twisted nematic liquid-crystal displays," J. Appl. Phys. 70(10),5346-5340 (1991).

[6] H. De Vleeschouwer, B. Verweire, K. D'Have, and H. Zhang, "Electrical and Optical Measurements of the Image Sticking Effect in Nematic LCD'S," Mol. Cryst. Liq. Cryst. 331(1), 567-574 (1999).

[7] H. De Vleeschouwer, F. Bougrioua, and H. Pauwels, "Importance of Ion Transport in Industrial LCD Applications, Mol. Cryst. Liq. Cryst.," 360(1), 29-39 (2001).

[8] D. Xu, F. Peng, H. Chen, J. Yuan, S.-T. Wu, M.-C. Li, S.-L. Lee, and W.-C. Tsai, "Image sticking in liquid crystal displays with lateral electric fields," J. Appl. Phys. 116(19), 193102 (2014).

[9] H. De Vleeschouwer, A. Verschueren, F. Bougrioua, R. van Asselt, E. Alexander, S. Vermael, K. Neyts, and H. Pauwels, "Long-term Ion Transport in Nematic Liquid Crystal Displays," Jpn. J. Appl. Phys. 40(Part 1, Number 5A), 3272-3276 (2001).

[10] K. H. Yang, "Charge retention of twisted nematic liquid-crystal displays," J. Appl. Phys. 67(1), 36-39 (1990).

[11] N. Sasaki, "A New Measurement Method for Ion Density in TFT-LCD Panels," Mol. Cryst. Liq. Cryst. 367(1), 671-679 (2001).

[12] S. Murakami and H. Naito, "Charge Injection and Generation in Nematic Liquid Crystal Cells," Jpn. J. Appl. Phys. 36(Part 1, Number 2), 773-776 (1997).

[13] S. Naemura and A. Sawada, "Ion Generation in Liquid Crystals under Electric Field," Mol. Cryst. Liq. Cryst. 346(1), 155-168 (2000).

[14] N. A. J. M. Van Aerle, "Influence of Polyimide Orientation Layer Material on the Liquid Crystal Resistivity in LCDs," Mol. Cryst. Liq. Cryst. 257(1), 193-208 (1994).

[15] K. Neyts, S. Vermael, C. Desimpel, G. Stojmenovik, R. van Asselt, A. R. M. Verschueren, D. K. G. de Boer, R. Snijkers, P. Machiels, and A. van Brandenburg, "Lateral ion transport in nematic liquid-crystal devices," J. Appl. Phys. 94(6), 3891-3896 (2003).

[16] M. Yamashita and Y. Amemiya, "Drift Mobility of Positive Ions in Nematic MBBA at Low Electric Field," Jpn. J. Appl. Phys. 17(9), 1513-1517 (1978).

[17] V. Novotny, "Measurement of mobilities of particles in liquids by optical and electrical transients," J. Appl. Phys. 50(4), 2787-2794 (1979).

[18] A. Sugimura, N. Matsui, Y. Takahashi, H. Sonomura, H. Naito, and M. Okuda, "Transient currents in nematic liquid crystals," Phys. Rev. B 43(10), 8272-8276 (1991).

[19] H. Naito, M. Okuda, and A. Sugimura, "Transient discharging processes in nematic liquid crystals," Phys. Rev. A 44(6), R3434-3497 (1991).

[20] H. Naito, K. Yoshida, and M. Okuda, "Transient charging current in nematic liquid crystals," J. Appl. Phys. 73(3), 1119-1125 (1993).

[21] C. Colpaert, B. Maximus, and A. De Meyere, "Adequate measuring techniques for ions in liquid crystal layers," Liq. Cryst. 21(1), 133-142 (1996).

[22] A. Sawada, A. Manabe, and S. Nameura, "A Comparative Study on the Attributes of Ions in Nematic and Isotropic Phases," Jpn. J. Appl. Phys. 40(Part 1, Number 1), 220-224 (2001).

[23] M. Sierakowski, "Ionic interface-effects in electro-optical LC-cells," Mol. Cryst. Liquid Cryst. 375 (1), 659–677 (2002).

[24] Y. Garbovskiy and I. Glushchenko, "Nano-Objects and Ions in Liquid Crystals: Ion Trapping Effect and Related Phenomena," Crystals 5(4), 501-533 (2015).

[25] S. Kumar, Liquid Crystals: Experimental Studies of Physical Properties and Phase Transitions, (Cambridge University Press: Cambridge, UK, 2000).

[26] P. Keller, L. Liebert, Liquid crystal synthesis for physicists. In Liquid Crystals; Supplement 14, Ed. L. Liebert, (Academic Press: New York, NY, USA, 1978; pp. 20–75.)

[27] J. L. Haberfeld, E. C. Hsu, J.F. Johnson, "Liquid crystal purification by zone refining," Mol. Cryst. Liquid Cryst. 24(1-2), 1–5 (1973).

[28] F. Gaspard, R. Herino, F. Mondon, "Low Field Conduction of Nematic Liquid Crystals Studied by Means of Electrodialysis", Mol. Cryst. Liquid Cryst. 24(1-2), 145–161 (1973).

[29] Y. Garbovskiy and I. Glushchenko, "Ion trapping by means of ferroelectric nanoparticles, and the quantification of this process in liquid crystals," Appl. Phys. Lett. 107(4), 041106 (2015).

[30] R. Basu and A. Garvey, "Effects of ferroelectric nanoparticles on ion transport in a liquid crystal," Appl. Phys. Lett. 105(15), 151905 (2014).

[31] Y.-S. Ha, H.-J. Kim, H.-G. Park, and D.-S. Seo, "Enhancement of electro-optic properties in liquid crystal devices via titanium nanoparticle doping," Opt. Express 20(6), 6448-6455 (2012).

[32] C.-W. Lee and W.-P. Shih, "Quantification of ion trapping effect of carbon nanomaterials in liquid crystals," Mater. Lett. 64(3), 466-668 (2010).

[33] H. Y. Chen, W. Lee, and N. A. Clark, "Faster electro-optical response characteristics of a carbon-nanotube-nematic suspension," Appl. Phys. Lett. 90(3), 033510 (2007).

[34] R. Basu, "Effect of carbon nanotubes on the field-induced nematic switching," Appl. Phys. Lett. 103(24), 241906 (2013).

[35] R. Basu, "Effects of graphene on electro-optic switching and spontaneous polarization of a ferroelectric liquid crystal," Appl. Phys. Lett. 105(11), 112905 (2014).

[36] R. Basu, A. Garvey, and D. Kinnamon, "Effects of graphene on electro-optic response and ion-transport in a nematic liquid crystal," J. Appl. Phys. 117(7), 074301 (2015).

[37] P.-W. Wu and W. Lee, "Phase and dielectric behaviors of a polymorphic liquid crystal doped with graphene nanoplatelets," Appl. Phys. Lett. 102(16), 162904 (2013).

[38] P.-C Wu, L.N. Lisetski, and W. Lee, "Suppressed ionic effect and low-frequency texture transitions in a cholesteric liquid crystal doped with graphene nanoplatelets," Opt. Express 23(9), 11195-11204 (2015).

[39] D. P. Singh, S. K. Gupta, T. Vimal, and R. Manohar, "Dielectric, electro-optical, and photoluminescence characteristics of ferroelectric liquid crystals on a graphene-coated indium tin oxide substrate," Phys. Rev. E 90(2), 022501 (2014).

[40] W. Lee, C.-Y. Wang, Y.-C. Shih, "Effects of carbon nanosolids on the electro-optical properties of a twisted nematic liquid-crystal host," Appl. Phys. Lett. 85(4), 513 (2004).

[41] R. K. Shukla, K. K. Raina, and W. Haase, "Fast switching response and dielectric behavior of fullerene/ferroelectric liquid crystal nanocolloids," Liq. Cryst. 41(12), 1726-1732 (2014).

[42] R. Basu and A. Lee, "Ion trapping by the graphene electrode in a graphene-ITO hybrid liquid crystal cell"; Applied Physics Letters 111(16), 161905 (2017).

[43] R. Basu and L. Atwood, "Reduced ionic effect and accelerated electro-optic response in a 2D hexagonal boron nitride planar-alignment agent based liquid crystal device", Optical Materials Express 9(3), 1441-1449 (2019).

[44] Y. Garbovskiy, “Kinetics of Ion-Capturing/Ion-Releasing Processes in Liquid Crystal Devices Utilizing Contaminated Nanoparticles and Alignment Films,” Nanomaterials 8(2), 59(2018).

[45] C. Kohout, C. Santi, L. Polito Anisotropic gold nanoparticles in biomedical applications. Int. J. Mol. Sci. 19(11), 3385 (2018).

[46] Dana M Samhadaneh, Siwei Chu, Dusica Maysinger; Ursula Stochaj, “How could gold nanourchins be applied in the clinic?” Nanomedicine 15(9), 829-832, (2020).

[47] P. G. De Gennes and J. Prost, The Physics of Liquid Crystals (Oxford University, 1994).

[48] M. Imai, H. Naito, M. Okuda, M. Okuda, and A. Sugimura, Jpn. J. Appl. Phys., Part 1 33, 3482 (1994).

[49] M. Imai, H. Naito, M. Okuda, and A. Sugimura, Molecular Crystals and Liquid Crystals Science and Technology. Section A. 259, 37 (1995).

[50] M. Imai, H. Naito, M. Okuda and A. Sugimura, Jpn. J. Appl. Phys., Part 1 34, 3170 (1995).

[51] R. Basu, L. Atwood, G. Sterling, “Dielectric and electro-optic effects in a nematic liquid crystal doped with h-BN flakes", Crystals 10(2), 123 (2020).

[52] L M. Blinov and V. G. Chigrinov, Electro-optic Effects in Liquid Crystal Materials (Springer-Verlag, New York, 1996).

[53] D. Demus, J. Goodby, G. W. Gary, H.W. Spiess, and V. Vill, Physical Properties of Liquid Crystals (Wiley VCH,Weinheim, Germany, 1999).